

RESEARCH ARTICLE

Development of a novel automatable fabrication method based on electrospinning co electrospaying for rotator cuff augmentation patches

Sergi Rey-Vinolas^{1,2}, Oscar Castaño^{1,2,3,4}, Leonardo Ruiz-Macarrilla⁵, Xavier Llorens^{6,7}, José M. Mora^{6,7}, Elisabeth Engel^{1,2,8*}, Miguel A. Mateos-Timoneda^{1,2,8*}

1 Biomaterials for Regenerative Therapies, Institute for Bioengineering of Catalonia (IBEC), The Barcelona Institute of Science and Technology (BIST), Barcelona, Spain, **2** CIBER en Bioingeniería, Biomateriales y Nanomedicina (CIBER-BBN), Madrid, Spain, **3** Serra Hunter Fellow, Electronics and Biomedical Engineering Department, University of Barcelona (UB), Barcelona, Spain, **4** Bioelectronics Unit and Nanobioengineering Lab., Institute for Nanoscience and Nanotechnology of the University of Barcelona (IN2UB), Barcelona, Spain, **5** Servei de C.O.T., Hospital Universitari Germans Trias i Pujol, Badalona, Spain, **6** Fundació Joan Costa Roma, Consorci Sanitari de Terrassa, Terrassa, Spain, **7** Servei de C.O.T., Hospital de Terrassa, Consorci Sanitari de Terrassa, Terrassa, Spain, **8** Department of Materials Science and Metallurgical Engineering, EEBE campus, Technical University of Catalonia (UPC), Barcelona, Spain

* eengel@ibecbarcelona.eu (EE); mamateos@ibecbarcelona.eu (MAM)



OPEN ACCESS

Citation: Rey-Vinolas S, Castaño O, Ruiz-Macarrilla L, Llorens X, Mora JM, Engel E, et al. (2019) Development of a novel automatable fabrication method based on electrospinning co electrospaying for rotator cuff augmentation patches. *PLoS ONE* 14(11): e0224661. <https://doi.org/10.1371/journal.pone.0224661>

Editor: Benedetto Marelli, Massachusetts Institute of Technology, UNITED STATES

Received: November 30, 2018

Accepted: October 18, 2019

Published: November 14, 2019

Copyright: © 2019 Rey-Vinolas et al. This is an open access article distributed under the terms of the [Creative Commons Attribution License](https://creativecommons.org/licenses/by/4.0/), which permits unrestricted use, distribution, and reproduction in any medium, provided the original author and source are credited.

Data Availability Statement: All relevant data are within the manuscript and its Supporting Information files.

Funding: This study has been granted by The Obra Social La Caixa, (Tendon Tissue Engineering: A Helping Hand for Rotator Cuff Tears (BIOTENDON). RECERCAIXA 2013), a non-profit organization that funds research on health and social topics. Thus, The funders had no role in study design, data

Abstract

Rotator cuff tear is one of the most common shoulder diseases. Rotator cuff augmentation (RCA) is trying to solve the high retear failure percentage after the surgery procedures (20–90%). The ideal augmentation patch must provide a temporal mechanical support during the healing process. In this work, we proposed a simple method for the fabrication of synthetic RCA patches. This method combines the use of electrospaying to produce poly-L-lactic-co-ε-caprolactone (PLC) films in an organogel form and electrospinning to produce poly(lactic) acid (PLA) nanofibers. The device consists in a combination of layers, creating a multilayered construct, enabling the possibility of tuning its mechanical properties and thickness. Besides, both techniques are simple to escalate for industrial production. A complete characterization has been performed to optimize the involved number of layers and production time of PLC films and PLA nanofibers fabrication, obtaining a final optimal configuration for RCA devices. Structural, mechanical and suture properties were evaluated. Also, the possibility of surface functionalization to improve the bioactivity of the scaffold was studied, adding aligned electrospun PLA nanofibers on the surface of the device to mimic the natural tendon topography. Surface modification was characterized by culturing adult normal human dermal fibroblasts. Lack of toxicity was detected for material presented, and cell alignment shape orientation guided by aligned fibers, mimicking tendon structure, was obtained. Cell proliferation and protein production were also evaluated.

collection and analysis, decision to publish, or preparation of the manuscript.

Competing interests: The authors have declared that no competing interests exist.

Introduction

Rotator cuff augmentation (RCA) has become an increasing technique to prevent tendon retear after a surgery repair. Only in the United States 17 million people suffer diseases related to rotator cuff [1–3], and 75,000 repair procedures per year are performed [4,5]. Specially, in cases with large, massive and chronic tears, the retear failure incidence ranges from 20% to 90% depending on the case [6–9].

Different types of patches for RCA have been studied since the 90s [10] in order to improve tendon reattachment and healing process, especially in large tears and chronic failures. Among them, decellularized extracellular matrix (ECM) membranes from different donors (porcine, equine, and human) provide a temporal and suitable support for cells and a source of biochemical signals and proteins that can stimulate the tissue regeneration.

However, one of the principal issues of these biological membranes is the remaining DNA. Some studies have shown the negative effects that they can produce if the decellularization and washing steps are not fully complete [11], and their possible relation with immune/inflammatory responses [12,13]. Other concern about the use of ECM membranes are their fast body resorption, losing their mechanical supporting resistance at early healing stages [14].

As an alternative to ECM membranes without antigenicity and inflammatory issues, synthetic degradable patches based on biocompatible polymers have been postulated. Properties like degradation rate, mechanical properties, shape and geometry can be easily modulated using different polymers, concentrations and fabrication techniques. In addition, many studies have reported the possibility of loading the synthetic degradable patches with signaling growth factors and drugs for their controlled release promoting a faster healing [15,16]. Depending on the fabrication method, it is possible to mimic the porosity and morphology of biological ECM. Electrospinning and electro-spraying are techniques based on the same principle, the acceleration of a polymer solution through a syringe to a collector under a high electrical field to obtain micro/nano fibers and particles/films, respectively [17,18]. Electrospinning/electro-spraying are widely used techniques in tissue engineering and regenerative medicine to obtain ECM-like shaped scaffolds, for example in bone regeneration [19], or as a drug delivery system [20].

In this work, we present a methodology based on the combination of electrospinning and electro-spraying, to obtain synthetic and degradable patches for RCA. Electro-spraying allows the fabrication of organogel films of Poly-L-lactic-co- ϵ -caprolactone (PLC). Previously, our group reported the fabrication methodology and characterization of scaffolds made of Poly (lactic) acid/EtLac organogels [21]. According to the expertise of clinicians the RCA scaffold device should stay for eight weeks in the damaged tendon. The goal is to provide a temporal mechanical support sharing the loads demands and allow the diffusion of oxygen and nutrients through them to enhance the healing of the injured tendon, without the need of cell infiltration at the earlier stages. After degradation and during the process of remodeling, cells are expected to penetrate within the scaffold. PLC organogel films were selected for this application due to their nanofibrous morphology and degradation properties.

Random PLA nanofibers fabricated by electrospinning were alternated between the different electro-sprayed films to modulate the final desired mechanical properties of the RCA patches. This combination of semi-automated techniques will allow a large-scale patch production. The choice of PLA nanofibers as reinforcement not only affects the mechanical properties, but also its degradation products (i.e. lactate) influencing cell behavior [22,23].

Due to the high boiling temperature of EtLac (154°C) in comparison with other common further used for electro-spraying process, like Chloroform (61°C), or Trifluoroethanol (78°C), and the high pump rate, EtLac is not completely evaporated during the process making

possible to obtain a polymer film in the organogel form. On the other hand, the release of lactate has been proposed to improve angiogenesis, a crucial process for tendon regeneration [24]. Hence, we have tested the biological effect of aligned PLA nanofibers on the surface of the patch.

Materials and methods

Materials

Poly-L/DL lactic acid 95/5 (Purasorb PLDL, intrinsic viscosity 6.15 dl/g) (PLA), and Poly-L-lactic-co- ϵ -caprolactone 70/30 (Purasorb PLC 7015, inherent viscosity midpoint 1.5 dl/g) (PLC) were purchased from Purac Biomaterials (The Netherlands). Ethyl L-lactate (EtLac), and 2,2,2-trifluoroethanol (TFE) were purchased from Sigma-Aldrich and Panreac, respectively.

Production of PLC films and PLA nanofibers

Polymeric films were obtained by electrospinning using a conventional equipment. Briefly, PLC solution (15% w/v in EtLac) was prepared and loaded into a 10ml syringe. The pumping syringe rate was fixed at 10 mL/h through a metallic needle (Red 25G, Nordson EFD), connected to voltage (8 KV) for accelerating the polymeric solution to the grounded collector at 10–18 cm distance. The speed of the cylindrical collector was fixed at 90 rpm.

For the fabrication of PLA nanofibers, a PLA solution (4% w/w in TFE) was prepared and loaded into a 10 mL syringe. The pumping rates was fixed at 0.5 mL/h using the same needle of 25G. Distance between tip to collector was fixed at 10 cm, and collector speed was set at 90 rpm to obtain a random orientation of the nanofibers. To mimic tendon structure, aligned PLA nanofibers were also produced with the same parameters as random PLA fibers but increasing the rotator speed up to 1000 rpm. This layer was the base of the final construct. The followed protocol to produce fibers was similar to the described previously by the group [22,25].

Finally, the construct was immersed in a water bath facilitating water-solvent exchange and promoting polymers precipitation to obtain the final structure (Fig 1).

Mechanical properties

Tensile tests were performed in a Zwick/Roell BT1 FR0.5TN.D14 testing machine. Software used for data acquisition was the provided by the manufacturer, testXpert II V3.41. The assay

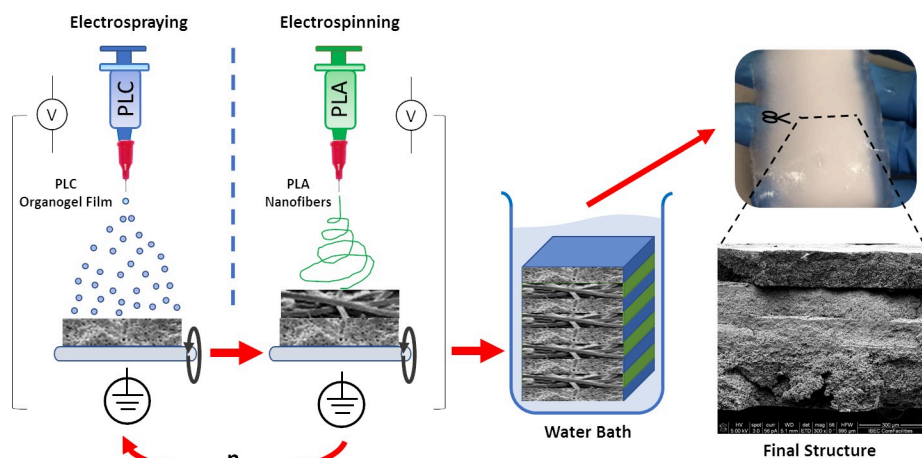


Fig 1. Schematic workflow representation of the RCA device fabrication.

<https://doi.org/10.1371/journal.pone.0224661.g001>

speed and preload of the sample were set at 10 mm/min and 0.1 N. All samples were cut into rectangles of 3x1 cm, clamping 1 cm of each sample side for testing.

Suture test was carried out with the same parameters as for the tensile tests. The sample dimensions were 3x1 cm, where the bottom side was clamped directly, and the upper side was attached the clamp through a suture retention loop (Polyglycolic acid USP 2 metric 5, Aragón). For wet condition, a 4L bath from Zwic/Roell was used filled with phosphate buffered solution (PBS) maintained at 37°C with a circulant water heater (E100, Lauda). Approached Young Modulus, and deformation at Yield Strength were evaluated. Due to the water bath set-up, deformation was assessed by the diagram displacement of testing machine.

Structure characterization by FE-SEM

The inner structure of the fabricated RCA devices was characterized by Field Emission Scanning Electron Microscopy (FE-SEM) using a Nova NanoSEM 230 microscope (FEI Corporation). Prior to visualization, samples were freeze dried (Alpha 1–4, Christ), and sputtered with 10 nm gold layer. Images were taken at 5 KV voltage with ETD detector. Fiber diameter was measured by ImageJ software from FE-SEM images obtained.

Biological characterization

Adult Normal Human Dermal fibroblasts (NHDF) (PromoCell, Germany) were used for the biological characterization. NHDF were cultured in Dulbecco's Modified Eagle Medium (DMEM), supplemented with 1% L-Glutamine, 1% Penicillin/Streptomycin, and 10% Fetal Bovine Serum (FBS), all purchased from Thermo Fischer Scientific (Massachusetts, USA). Cell culture media was changed every two/three days and the cells were used in passages 3–6 for all the experiments.

Two different conditions were studied: in the first condition, RCA devices with aligned fibers on the surface were tested; whereas in the second condition, the RCA devices do not present aligned fibers on their surface. Scaffolds were cut into squares of 1x1 cm for the biological characterization assays. RCA devices without cells were used as negative controls for the experiments.

Cytotoxicity assays

Cytotoxicity was evaluated indirectly using conditioned media assay. In parallel, 10×10^3 NHDFs were seeded into 24 well plate, and scaffolds with/without PLA aligned fibers (1x1cm) were immersed in cell culture media into different 24 well plate and incubated for 24 hours. Then, the media from NHDFs was changed for conditioned media and incubated for 24 hours more. After this time, live/dead staining, based on Calcein-AM and propidium iodide (both from Sigma Aldrich), was performed. Images were taken at 10x augments with DM IRBE Leica microscope. For quantitative LDH cytotoxic evaluation, same procedure with conditioned media was used prolonged in time. At 1, 3, 5, 7 and 9 days, conditioned media in contact with materials was transferred to NHDFs wells, and material wells were replaced with new media. One condition of NHDFs incubated with media that was not in contact with materials was used as a control. LDH absorbance was read following the manufacturer's protocol (Roche), at 492nm with a reference at 680nm with a microplate reader (Benchmark Plus, BioRad). Results are expressed as an absorbance percentage of conditioned media from materials condition over control condition.

Cell metabolic assay

Alamar blue (Thermo Fischer Scientific) assay was selected for cell metabolic assay as non-destructive assay. Both conditions, with and without aligned fibers on top, were evaluated. Scaffolds of 1x1 cm in size were cut and placed into 24 well plates with ultra-low attachment surface treatment (Corning). 40×10^3 NHDFs were seeded on top of the scaffolds. Cell metabolic activity was measured at days 2, 5, 9 and 14.

Total protein quantification

Total protein amount was quantified at day 3, 7 and 14 with a Pierce BCA protein assay kit (Thermo Fischer Scientific). Samples of 1x1 cm were cut and placed in ultra-low attachment 24 well plates (Corning). 30×10^3 NHDFs were seeded on each sample in 1 mL of cell culture media. Triplicate of both conditions, scaffolds with and without aligned fibers on the surface, were evaluated. For each condition, blanks were added corresponding to scaffolds without cells to subtract the background signal. Protein extraction was made using mammalian protein extraction reagent (Thermo Fischer Scientific), after rinsed samples 3 times in PBS and freeze them at -80°C . The protocol followed for the quantification was the supplied one by the manufacturer. Briefly, samples were thawed, and the surface scraped. 25 μL of samples were added for triplicate in 96 wells plate. After that, 200 μL of working reagent supplied with the kit were added. A standard curve was prepared at the same time. The wells plate was incubated during 30 minutes at 37°C , following by 5 minutes at room temperature before assessing the absorbance at 562 nm with an Infinite M200 PRO microplate reader (Tecan).

Cell morphology by confocal fluorescence images

Samples with cells seeded were incubated for 3 and 7 days, at each time point, samples were fixed with 4% Paraformaldehyde (PFA) for 10 minutes. Afterwards, they were rinsed thrice with PBS, and permeabilized with 0.5% Triton X-100 for 5 minutes. Phalloidin (Phalloidin-TRITC) and DAPI (both from Sigma Aldrich) were used for actin and nuclei staining. Images were taken at 10X augments with LSM 800 Zeiss confocal microscope. Actin fiber orientation histograms were obtained with Directionality ImageJ plugin (<https://imagej.net/Directionality>) from Phalloidin stained images.

Statistics

Data are presented as mean \pm standard deviation of the replicates. Statistical significance was assessed with analysis of variance (ANOVA) with a level of significance of $P < 0.05$. Student's *t*-test ($P < 0.05$) was applied at fiber integration into PLC films and suture test when only two conditions were compared.

Results and discussion

In this study, the fabrication process of patches for RCA is presented. These RCA devices are made of PLC films by electrospinning and PLA nanofibers by electrospinning. The combination of these techniques simplifies the fabrication process just changing parameters like voltage, distance and syringe (polymer solution and concentration) in the same device. Thus, the scale-up of RCA patches is straightforward facilitating laboratory to clinic translation. The wide range of techniques and companies that provide specific electrospinning equipment and solutions for research laboratories and medical device industries is another advantage [26,27].

Production of organogel PLC films by electro spraying and PLA fibers addition by electro spinning

The inner microstructure of PLC/EtLac organogels films produced by electro spraying after solvent exchange in water was characterized by FE-SEM [21]. In Fig 2, it is possible to appreciate the fibrous morphology of the film cross section, which validates electro spraying as a new method to obtain a fibrous structure of the PLC films.

The addition of PLA nanofibers to the PLC organogel films was a crucial step to reinforce the mechanical properties of the patch, achieving the optimal ones for the RCA application. For this purpose, three different fiber deposition time points were tested (10, 20 and 30 minutes). FE-SEM analysis of the inner structure of the devices shows no differences in terms of fiber adhesion and density (Fig 3A, 3B and 3C). However, a significant increment of the approached Young's Modulus (14 MPa) was obtained for the 30 minutes condition, in contrast to the 6 MPa obtained for the rest of conditions (Fig 3D and 3E). As expected, the final thickness of the device was not affected by the length of the deposition. Fiber diameter for random PLA fibers was $1.35 \pm 0.52 \mu\text{m}$ averaged diameter.

In order to introduce PLA nanofibers between the PLC films and to evaluate the different production times, a sequential alternated production of film/fibers/film was studied. Two different conditions (30 and 60 minutes PLC film production) were tested, whereas the production time of PLA fibers was set constant (20 minutes, as an intermediate time point).

A complete integration of the fibers for both conditions is observed in (Fig 4A and 4B). However, only is possible to identify union regions of the two films produced, where the PLA fibers are embedded between both PLC films. No significant differences for the approached Young's Moduli were obtained (around 5 MPa for both conditions) (Fig 4C). In contrast, significant differences were observed increasing PLC film time production: from 0,3 mm for the 30/20/30 condition to 0,65 mm for the 60/20/60 condition (Fig 4D). These results suggest that the PLA fibers layers only affects the mechanical properties of the device, while the PLC film layers has an effect in thickness and the main inner porosity microstructure of the RCA patch.

Thus, the combination different times of production and number of layers of PLC films and PLA fibers allows the fine tuning of the mechanical properties and geometry of the patch.

Determination of PLC films and PLA fibers layers number

Consequently, different number of PLC films and PLA fibers layers sequentially produced have been studied with the aim to reach similar mechanical properties to other devices reported in the bibliography [28,29]. Three conditions were characterized increasing the number of PLA fibers (see nomenclatures in Table 1). Fig 5A shows the Young Modulus of the different samples. Significant differences were obtained with lower Young's Modulus at the range

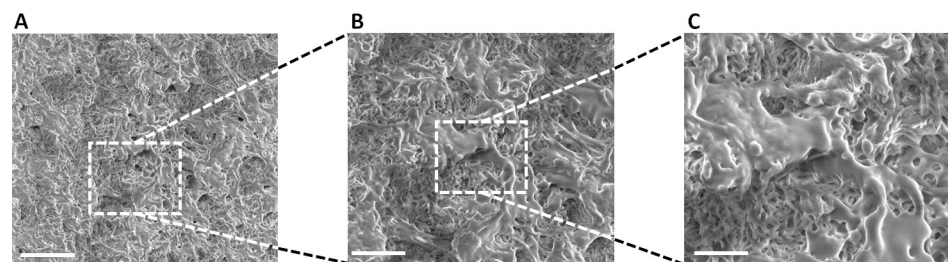


Fig 2. FE-SEM images from PLC films cross section. Inner structure of the PLC organogel film obtained by electro spraying, from A) 5000, B) 6000 and C) 12000 augments. (Scale bars corresponds to 20, 10 and 5 microns for A, B and C, respectively).

<https://doi.org/10.1371/journal.pone.0224661.g002>

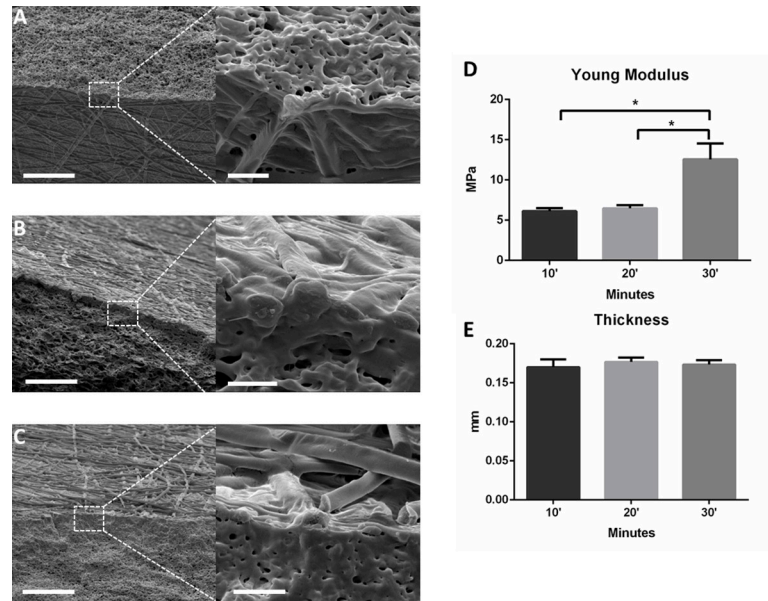


Fig 3. Different production times of electrospun PLA fibers added on a PLC organogel film. FE-SEM cross section images of production PLA fibers on the organogel PLC film during A) 10 minutes, B) 20 minutes and C) 30 minutes (scale bars = 30 microns. Inserts: scale bar = 3 microns). D) Young Modulus and E) thickness measurements of the different conditions (n = 3, *P<0.05).

<https://doi.org/10.1371/journal.pone.0224661.g003>

of 18MPa for the 2L30/40 condition against 3L30/40 condition (range of 30MPa), no significant differences were obtained between 3L30/40 and 4L35/40. The axial stiffness (calculated from Young Modulus [30]) of the devices were 6.40, 10.54 and 17.34 N/mm for 2L30/40, 3L30/40 and 4L35/40, respectively. Fig 5B. shows the thickness of the three different devices. Although 3L30/40 has similar mechanical properties as 4L35/40, its thickness is around 1.5-fold lower (0.4 and 0.63 mm, respectively). The thickness of the devices can be affected by

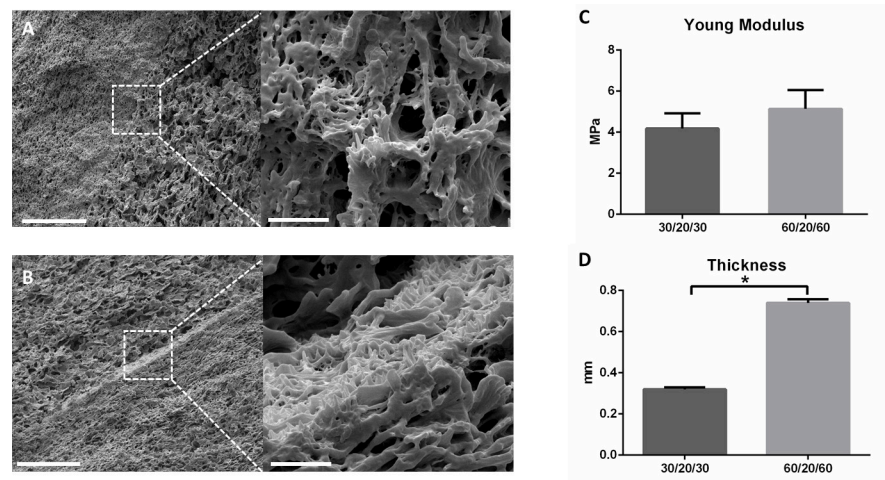


Fig 4. Embedded PLA fibers between two PLC films FE-SEM cross-section images. A) 30 minutes and B) 60 minutes of PLA fibers production (scale bar = 30 microns. Inserts: scale bar = 3 microns). C) Young Modulus and D) thickness measurements of the different conditions (n = 3, *P<0.05).

<https://doi.org/10.1371/journal.pone.0224661.g004>

Table 1. Nomenclatures relation to the number of layers and time of layer production for each construct studied.

N° PLC film	PLC film Production Time (min/layer)	N° PLA fibers	PLA fibers Production Time (min/layer)	Nomenclature
3	30	2	40	2L30/40
4	30	3	40	3L30/40
5	35	4	40	4L35/40
5	35	4	40	F4L35/40*

*Condition with extra 30 minutes of aligned electrospun PLA fibers.

<https://doi.org/10.1371/journal.pone.0224661.t001>

the number of layers and deposition time. For this reason, PLC films deposition time was increased in 5 minutes and an extra PLA fiber layer was added to maintain the mechanical resistance and increase the thickness (4L35/40 condition). This thickness value of 0.63 mm is similar to RCA commercial patches [31]. SEM images of cross sections were taken for 4L35/40 condition (Fig 5C). The different layers (PLC films and PLA fibers) can be easily identified. Deformation at Yield Strength measured for the three conditions did not show significant differences. As shown in S1A Fig, all conditions are around 2–4% of deformation. S1B Fig show representative elastic region strain-stress curves of the three conditions. This range is compatible with the range of tendon deformation, which at 4% starts the microscopy tearing of tendon fibers [32].

Suture test

A suture test was designed to evaluate the patch behavior [28,33,34]. Two different conditions were evaluated, dry conditions at RT and wet conditions (PBS) at 37°C. As expected, a

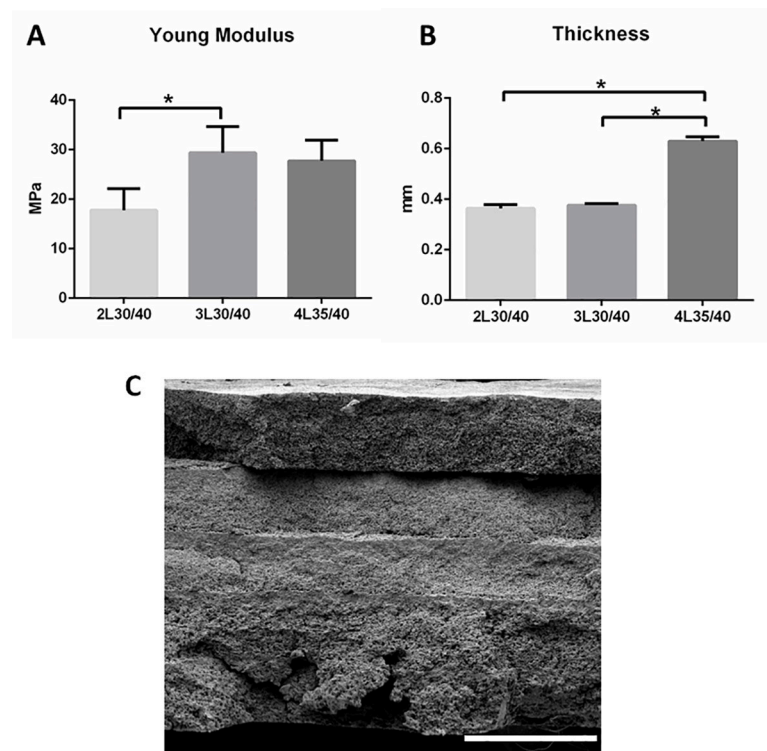


Fig 5. A) Young Modulus and B) thickness measurement for the different conditions (n = 3, *P<0.05). C) FE-SEM images of the inner structure of 4L35/40 (scale bar = 300 microns).

<https://doi.org/10.1371/journal.pone.0224661.g005>

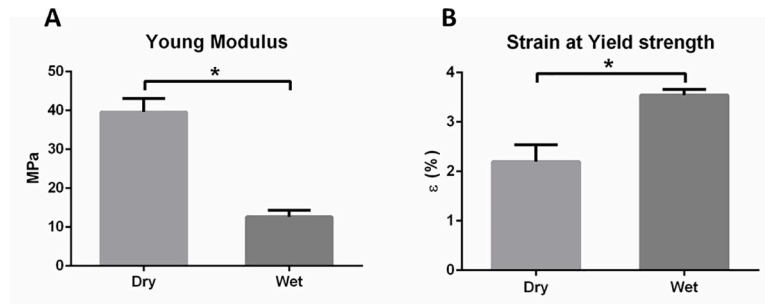


Fig 6. A) Young Modulus and B) Strain at Yield strength obtained for dry and wet conditions of suture assay of 4L35/40 (n = 3, *P<0.05).

<https://doi.org/10.1371/journal.pone.0224661.g006>

significant decrease of Young's Modulus (Fig 6A) and an increase of the strain at the yield strength were obtained for the wet conditions (Fig 6B), due to the higher temperature and liquid media effect. Temperature, in particular for polymers, is an important factor to consider during the material characterization, because it affects directly the mechanical properties and the performance of devices. Despite mechanical properties of patch and suture retention, the tendon-to-bone fixation technique and the patch features plays a crucial role in biomechanics and stability [6,35].

Biological characterization

An ideal RCA patch fabrication method should allow the surface modification to introduce chemical and physical signals on the device to better mimic the tendon structure and bioactivity [36,37]. In this way, electrospinning was also used to produce aligned nanofibers on the surface of the scaffold with $1.47 \pm 0.39 \mu\text{m}$ averaged diameter, mimicking the tendon collagen fibers. Tendon has a hierarchical structure organization based on collagen fibers, known as fibrils, aligned to the long axis of the tendon closely packed together [38]. It is known that aligned patterns affect cells phenotype [39]. Yin et al. found that aligned electrospun fibers promote tendon stem/progenitor cells differentiation to tendon linages [40]. This topography effect has been confirmed also with *in vivo* assays, where random fibers induced Mesenchymal Stem Cells (MSCs) to bone lineage and aligned fibers to tendon lineage [41]. Fee et al. showed that genes related to actin production, polymerization and focal adhesions were upregulated when fibroblast were seeded on aligned electrospun fibers [42]. Due to that, one condition with aligned PLA fibers on the surface (noted as F4L35/40 at Table 1) was added to the previous condition selected (4L35/40) for the biological characterization. Mechanical properties obtained for F4L35/40 condition were no significantly different from 4L35/40 (28.5MPa approached Young Modulus). FE-SEM images of the surface for the fibers condition were taken (Fig 7A). The effect of the surface pattern to cell metabolic activity and protein production was studied comparing the condition of 4L35/40 and F4L35/40 for all the biological assays.

First step was to check whether scaffolds had any toxicity effect to NHDFs cultures, for example, as a result of solvent residues after precipitation process. In Fig 7B, 7C and 7D, cell viability shows above 90% of cells are alive (green cells alive, red cells dead). Thus, for the LDH cytotoxic assay prolonged in time, until 9 days (S2 Fig), lack of toxicity was observed for both conditions.

Cell metabolic assay on the scaffold surface was evaluated seeding NHDFs on 4L35/40 and F4L35/40. Results are shown as a percentage of the measure done after 3 hours of seeding. No

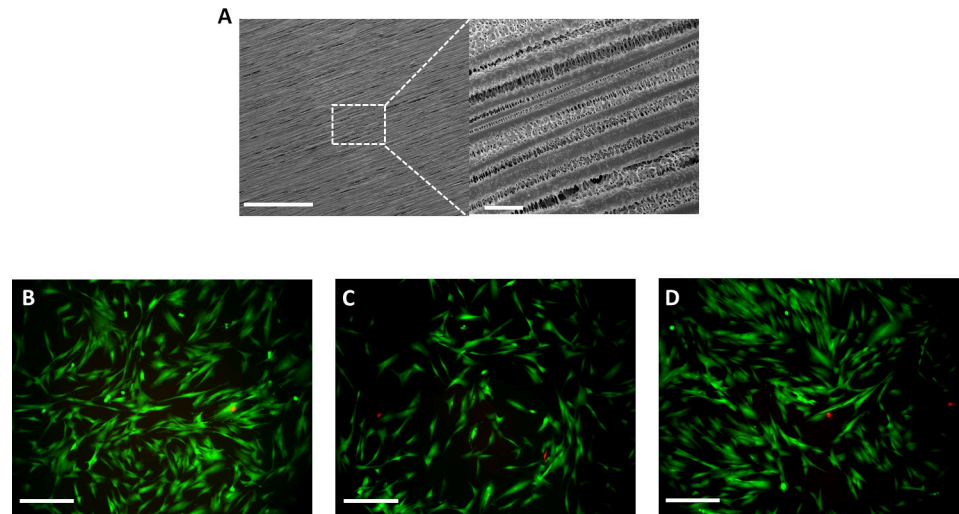


Fig 7. A) FE-SEM images of the surface modification adding electrospun PLA aligned fibers F4L35/40 (scales bar = 300 microns. Insert: scale bar 5 microns). B) Qualitative live/dead assay using the conditioned media from control condition (TCP), C) 4L35/40 and D) F4L35/40 (scale bar = 100 microns).

<https://doi.org/10.1371/journal.pone.0224661.g007>

significant differences were obtained between both conditions for all the measured time points for the cell metabolic assay (Fig 8A). Both conditions have a positive linear slope during the assay. It has already been shown that there is no correlation between fibers direction and fibroblasts proliferation [43].

The amount of proteins produced by cells was also quantified for both conditions (Fig 8B). No significant differences were obtained in protein production between F4L35/40 and 4L35/40 conditions from days 3 to 14. Even though, the benefits for tendon/ligament applications of fiber alignment on ECM proteins production have been previously reported. C. Hunt et al. reported more collagen production by fibroblasts seeded on aligned fibers than seeded on random orientation fibers [44]. Also Thomas K. et al. found an increase of production of Collagen I at day 7 and Collagen III at day 14 by MSCs seeded on aligned fibers than random [45]. In addition, Wang et al. showed that aligned culture produce also an aligned collagen matrix, like tendon structure [46]. More assays are needed to study the biological effect of adding aligned fibers on the RCA device, and their benefits. The possibility of modulating the production of ECM proteins like collagen type III and I, which are characteristics of the second and third

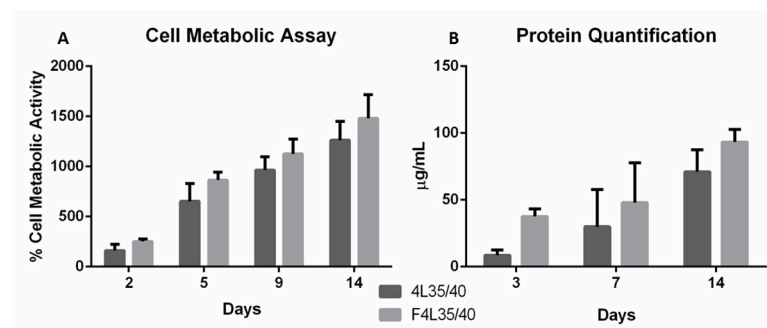


Fig 8. A) Cell metabolic activity, data is referenced in percentage respect to the values obtained at 3 hours (n = 6, *P < 0.05). B) Total protein quantification (n = 3, *P < 0.05).

<https://doi.org/10.1371/journal.pone.0224661.g008>

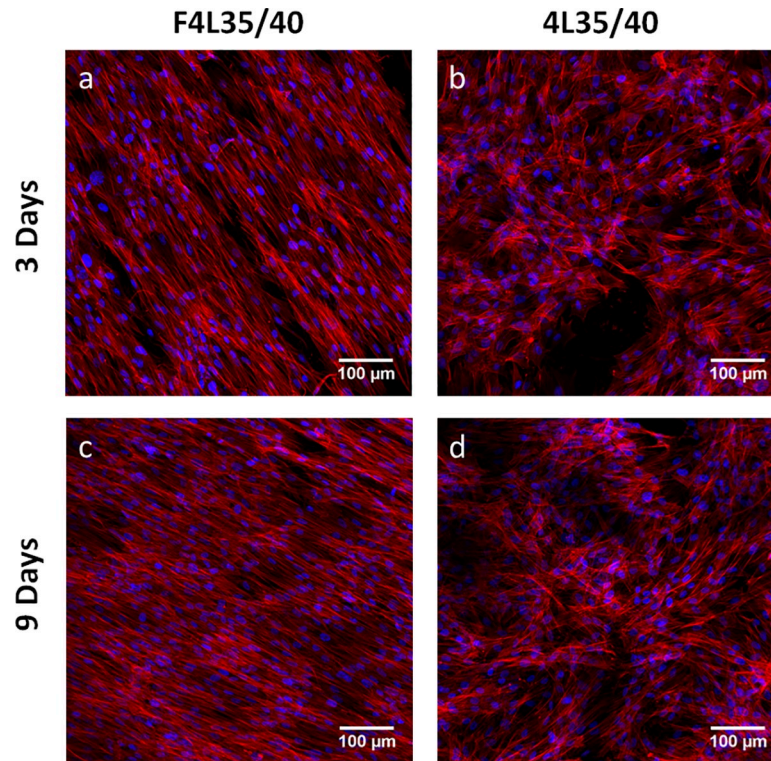


Fig 9. Confocal images of NHDFs A) after 3 days cultured on F4L35/40, B) after 3 days cultured on 4L35/40, C) after 7 days cultured on F4L35/40 and D) after 7 days cultured on 4L35/40. Actin stained with Phalloidin-TRITC (red) and nuclei stained with DAPI (blue).

<https://doi.org/10.1371/journal.pone.0224661.g009>

tendon healing stages [47,48], by the surface pattern might be a way to enhance the tendon healing process.

Finally, the effect of the aligned fibers condition in morphogenesis was also studied by fluorescent confocal images. It is known that aligned patterns also affect the cells' morphology following fibers orientation [49]. At Fig 9, it is possible to observe the effect of surface pattern to cell morphology after 3 and 7 days of culture. After 3 days of culture, it is possible to appreciate the aligned morphology of NHDFs seeded on F4L35/40 (Fig 9A) in contrast with rounded shape morphology for NHDFs seeded on 4L35/40. After 7 days, both conditions are completely colonized by NHDFs, maintaining their morphology observed at day 3 (Fig 9C and 9D). Histograms of actin fibers orientation were obtained from Phalloidin staining from confocal images of NHDFs (S3A and S3B Fig). As it is shown, the aligned fiber pattern had a contact-guide effect on the cells after 7 days cultured on F4L35/40 (S3C Fig), with a Full width at half maximum of approximately 22° (gaussian fitted curve). No actin orientation was detected for NHDFs cultured on 4L35/40 (S3D Fig). Therefore, these results supported with the bibliography findings, suggest that aligned fibers patterns affect their morphology and could influence the ECM topography mimicking the tendon tissue structure, and could be a promising strategy to improve surface bioactivity for a rotator cuff augmentation device.

Conclusions

Here we presented a novel method to produce organogel PLC/EtLac films by electrospraying, and also characterized their mechanical properties improvement by the addition of PLA fibers using electrospinning. Combining the two methods made possible the fabrication of a

degradable synthetic composite patch for RCA, obtaining the optimal configuration, 4L35/40 condition, for a rotator cuff augmentation device application. Moreover, surface patch pattern has been modified by adding electrospun aligned PLA fibers mimicking tendon structure to promote the successful biological response, achieving a cell alignment morphology like tendon tissue. *in vivo* experiments are needed to confirm the adequate performance of this new device for tendon applications. However, the scale-up for industrial production looks promising due to the simplicity and versatility of the set-up here proposed.

Supporting information

S1 Fig. A) Deformation at Yield Strength (n = 3, *P<0.05). B) Representative Strain-Stress curves adjusted to highlight elastic regions.
(TIF)

S2 Fig. Results obtained for the cytotoxicity assay with conditioned media. Values are normalized by the control condition (cells with media that were not in contact with materials). (n = 4, *P<0.05).
(TIF)

S3 Fig. Actin staining of NHDFs after 7 days cultured on F4L35/40 A), and on 4L35/40 B). Fiber orientation histogram of NHDFs actin staining after 7 days cultured on F4L35/40 C), and on 4L35/40 D).
(TIF)

S1 File. RCA device fabrication protocol.
(DOCX)

Author Contributions

Conceptualization: Leonardo Ruiz-Macarrilla, Xavier Llorens, José M. Mora, Miguel A. Mateos-Timoneda.

Data curation: Sergi Rey-Vinolas, Miguel A. Mateos-Timoneda.

Formal analysis: Sergi Rey-Vinolas, Oscar Castaño, José M. Mora, Miguel A. Mateos-Timoneda.

Investigation: Sergi Rey-Vinolas, Leonardo Ruiz-Macarrilla, Xavier Llorens, José M. Mora.

Methodology: Sergi Rey-Vinolas, Oscar Castaño, Leonardo Ruiz-Macarrilla, Xavier Llorens.

Project administration: José M. Mora.

Resources: Elisabeth Engel.

Supervision: Elisabeth Engel, Miguel A. Mateos-Timoneda.

Validation: Oscar Castaño, Leonardo Ruiz-Macarrilla, Elisabeth Engel.

Writing – original draft: Sergi Rey-Vinolas, Miguel A. Mateos-Timoneda.

Writing – review & editing: Oscar Castaño, José M. Mora, Elisabeth Engel, Miguel A. Mateos-Timoneda.

References

1. McElvany MD, McGoldrick E, Gee AO, Neradilek MB, Matsen FA. Rotator cuff repair: Published evidence on factors associated with repair integrity and clinical outcome. *Am J Sport Med.* 2015; 43: 491–500. <https://doi.org/10.1177/0363546514529644> PMID: 24753240
2. Fehring E V., Sun J, VanOeveren LS, Keller BK, Matsen FA. Full-thickness rotator cuff tear prevalence and correlation with function and co-morbidities in patients sixty-five years and older. *J Shoulder Elb Surg.* 2008; 17: 881–885. <https://doi.org/10.1016/j.jse.2008.05.039> PMID: 18774738
3. Yamaguchi K, Ditsios K, Middleton WD, Hildebolt CF, Galatz LM, Teefey SA. The Demographic and Morphological Features of Rotator Cuff Disease. A Comparison of Asymptomatic and Symptomatic Shoulders. *J Bone Jt Surg Am.* 2006; 88: 1699–1704. <https://doi.org/10.2106/jbjs.e.00835> PMID: 16882890
4. Ricchetti ET, Aurora A, Iannotti JP, Derwin KA. Scaffold devices for rotator cuff repair. *J shoulder Elb Surg.* 2012; 21: 251–265. <https://doi.org/10.1016/j.jse.2011.10.003> PMID: 22244069
5. Vitale MA, Vitale MG, Zivin JG, Braman JP, Bigliani LU, Flatow EL. Rotator cuff repair: An analysis of utility scores and cost-effectiveness. *J Shoulder Elb Surg.* 2007; 16: 181–187. <https://doi.org/10.1016/j.jse.2006.06.013> PMID: 17399623
6. Aurora A, Eng D, Mccarron JA, Van Den Bogert AJ, Gatica JE, Iannotti JP, et al. The biomechanical role of scaffolds in augmented rotator cuff tendon repairs. *J Shoulder Elb Surg.* 2012; 21: 1064–1071. <https://doi.org/10.1016/j.jse.2011.05.014> PMID: 21885301
7. Galatz LM, Ball CM, Teefey SA, Middleton WD, Yamaguchi K. The outcome and repair integrity of completely arthroscopically repaired large and massive rotator cuff tears. *J Bone Joint Surg Am.* 2004; 86–A: 219–24.
8. Gazielly DF, Gleyze P, Montagnon C. Functional and anatomical results after rotator cuff repair. *Clin Orthop Relat Res.* 1994; 43–53.
9. Harryman DT, Mack LA, Wang KY, Jackins SE, Richardson ML, Matsen FA. Repairs of the rotator cuff. Correlation of functional results with integrity of the cuff. *J Bone Joint Surg Am.* 1991; 73: 982–9. PMID: 1874784
10. France EP, Paulos LE, Harner CD, Straight CB. Biomechanical evaluation of rotator cuff fixation methods. *Am J Sports Med.* 1989; 17: 176–181. <https://doi.org/10.1177/036354658901700206> PMID: 2757125
11. Gilbert TW, Freund JM, Badylak SF. Quantification of DNA in Biologic Scaffold Materials. *J Surg Res.* 2009; 152: 135–139. <https://doi.org/10.1016/j.jss.2008.02.013> PMID: 18619621
12. Keane TJ, Londono R, Turner NJ, Badylak SF. Consequences of ineffective decellularization of biologic scaffolds on the host response. *Biomaterials.* 2012; 33: 1771–1781. <https://doi.org/10.1016/j.biomaterials.2011.10.054> PMID: 22137126
13. Walton BR, Bowman NK, Khatib Y, Murrell GAC. Restore Orthobiologic Implant: Not Recommended for Augmentation of Rotator Cuff Repairs. *J Bone Jt Surg.* 2007; 786–792. <https://doi.org/10.2106/JBJS.F.00315> PMID: 17403801
14. Ratcliffe A, Butler DL, Dymont NA, Cagle PJ, Proctor CS, Ratcliffe SS, et al. Scaffolds for Tendon and Ligament Repair and Regeneration. *Ann Biomed Eng.* 2015; 43: 819–831. <https://doi.org/10.1007/s10439-015-1263-1> PMID: 25650098
15. Prabhat A, Vernekar VN, Sanchez E, Laurencin CT. Growth factor delivery strategies for rotator cuff repair and regeneration. *Int J Pharm.* 2018; 544: 358–371. <https://doi.org/10.1016/j.ijpharm.2018.01.006> PMID: 29317260
16. Liu S, Qin M, Hu C, Wu F, Cui W, Jin T, et al. Tendon healing and anti-adhesion properties of electrospun fibrous membranes containing bFGF loaded nanoparticles. *Biomaterials.* 2013; 34: 4690–4701. <https://doi.org/10.1016/j.biomaterials.2013.03.026> PMID: 23541108
17. Sill TJ, von Recum HA. Electrospinning: Applications in drug delivery and tissue engineering. *Biomaterials.* 2008; 29: 1989–2006. <https://doi.org/10.1016/j.biomaterials.2008.01.011> PMID: 18281090
18. Bodnár E, Grifoll J, Rosell-Illompert J. Polymer solution electrospinning: A tool for engineering particles and films with controlled morphology. *J Aerosol Sci.* 2018; 125: 93–118. <https://doi.org/10.1016/j.jaerosci.2018.04.012>
19. Jang JH, Castano O, Kim HW. Electrospun materials as potential platforms for bone tissue engineering. *Adv Drug Deliv Rev.* 2009; 61: 1065–1083. <https://doi.org/10.1016/j.addr.2009.07.008> PMID: 19646493
20. Bock N, Dargaville TR, Woodruff MA. Electrospinning of polymers with therapeutic molecules: State of the art. *Prog Polym Sci.* 2012; 37: 1510–1551. <https://doi.org/10.1016/j.progpolymsci.2012.03.002>

21. Punet X, Levato R, Bataille I, Letourneur D, Engel E, Mateos-Timoneda MA. Polylactic acid organogel as versatile scaffolding technique. *Polym (United Kingdom)*. 2017; 113. <https://doi.org/10.1016/j.polymer.2017.02.056>
22. Álvarez Z, Castaño O, Castells AA, Mateos-timoneda MA, Planell JA, Engel E, et al. Neurogenesis and vascularization of the damaged brain using a lactate-releasing biomimetic scaffold. *Biomaterials*. 2014; 35: 4769–4781. <https://doi.org/10.1016/j.biomaterials.2014.02.051> PMID: 24636215
23. Álvarez Z, Mateos-timoneda MA, Hyro P, Castaño O, Planell JA, Perales JC, et al. The effect of the composition of PLA films and lactate release on glial and neuronal maturation and the maintenance of the neuronal progenitor niche. *Biomaterials*. 2013; 34. <https://doi.org/10.1016/j.biomaterials.2012.12.001> PMID: 23276659
24. Hu X-F, Feng Y, Xiang G, Lei W, Wang L. Lactic acid of PLGA coating promotes angiogenesis on the interface between porous titanium and diabetic bone. *J Mater Chemistry B*. 2018; 2274–2288. <https://doi.org/10.1039/c7tb03247a>
25. Mateos-timoneda MA, Castano O, Planell JA, Engel E. Effect of structure, topography and chemistry on fibroblast adhesion and morphology. *J Mater Sci Mater Med*. 2014; 1781–1787. <https://doi.org/10.1007/s10856-014-5199-z> PMID: 24668270
26. Persano L, Camposeo A, Tekmen C, Pisignano D. Industrial Upscaling of Electrospinning and Applications of Polymer Nanofibers: A Review. *Macromol Mater Eng*. 2013; 504–520. <https://doi.org/10.1002/mame.201200290>
27. Yu M, Dong R, Yan X, Yu G, You M, Ning X, et al. Recent Advances in Needleless Electrospinning of Ultrathin Fibers: From Academia to Industrial Production. *Macromol Mater Eng*. 2017. <https://doi.org/10.1002/mame.201700002>
28. Barber FA, Aziz-jacobo J. Biomechanical Testing of Commercially Available Soft-Tissue Augmentation Materials. *J Arthrosc Relat Surg*. 2009; 25: 1233–1239. <https://doi.org/10.1016/j.arthro.2009.05.012> PMID: 19896044
29. Derwin KA, Leigh DR, Iannotti JP. Commercial Extracellular Matrix Scaffolds for Rotator Cuff Tendon Repair. *J Bone Jt Surg*. 2006; 2665–2672.
30. Lacroix AS, Duenwald-kuehl SE, Lakes RS, Vanderby R. Relationship between tendon stiffness and failure: a metaanalysis. *J Appl Physiol*. 2013; 43–51. <https://doi.org/10.1152/jappphysiol.01449.2012> PMID: 23599401
31. Coons DA, Alan Barber F. Tendon graft substitutes—Rotator cuff patches. *Sports Med Arthrosc*. 2006; 14: 185–190. <https://doi.org/10.1111/ens.12096> PMID: 17135966
32. Wang C H. J. Mechanobiology of tendon. *J Biomech*. 2006; 39: 1563–1582. <https://doi.org/10.1016/j.jbiomech.2005.05.011> PMID: 16000201
33. Chaudhury S, Holland C, Thompson MS, Vollrath F, Carr AJ. Tensile and shear mechanical properties of rotator cuff repair patches. *J Shoulder Elb Surg*. 2012; 21: 1168–1176. <https://doi.org/10.1016/j.jse.2011.08.045> PMID: 22079767
34. Barber FA, Herbert MA, Coons DA. Tendon Augmentation Grafts: Biomechanical Failure Loads and Failure Patterns. *Arthrosc—J Arthrosc Relat Surg*. 2006; 22: 534–538. <https://doi.org/10.1016/j.arthro.2005.12.021> PMID: 16651164
35. Jung C, Spreiter G, Audigé L, Ferguson SJ, Flury M. Patch-augmented rotator cuff repair: influence of the patch fixation technique on primary biomechanical stability. *Arch Orthop Trauma Surg*. 2016; 136: 609–616. <https://doi.org/10.1007/s00402-016-2436-6> PMID: 26983721
36. Chainani A, Little D. Current Status of Tissue-Engineered Scaffolds for Rotator Cuff Repair. *Tech Orthop*. 2016; 31: 91–97. <https://doi.org/10.1097/BTO.000000000000168> PMID: 27346922
37. Patel S, Gualtieri AP, Lu HH, Levine WN. Advances in biologic augmentation for rotator cuff repair. *Ann N Y Acad Sci*. 2016; 1383: 97–114. <https://doi.org/10.1111/nyas.13267> PMID: 27750374
38. Voleti PB, Buckley MR, Soslowsky LJ. Tendon Healing: Repair and Regeneration. *Annu Rev Biomed Eng*. 2012; 14: 47–71. <https://doi.org/10.1146/annurev-bioeng-071811-150122> PMID: 22809137
39. Wang W, He J, Feng B, Zhang Z, Zhang W, Zhou G, et al. Aligned nanofibers direct human dermal fibroblasts to tenogenic phenotype in vitro and enhance tendon regeneration in vivo. *Nanomedicine*. 2016; 11: 1055–1072. <https://doi.org/10.2217/nnm.16.24> PMID: 27074092
40. Yin Z, Chen X, Chen JL, Shen WL, Hieu Nguyen TM, Gao L, et al. The regulation of tendon stem cell differentiation by the alignment of nanofibers. *Biomaterials*. 2010; 31: 2163–2175. <https://doi.org/10.1016/j.biomaterials.2009.11.083> PMID: 19995669
41. Yin Z, Chen X, Song H, Hu J, Tang Q, Zhu T, et al. Electrospun scaffolds for multiple tissues regeneration in vivo through topography dependent induction of lineage specific differentiation. *Biomaterials*. 2015; 44: 173–185. <https://doi.org/10.1016/j.biomaterials.2014.12.027> PMID: 25617136

42. Fee T, Surianarayanan S, Downs C, Zhou Y, Berry J. Nanofiber alignment regulates NIH3T3 cell orientation and cytoskeletal gene expression on electrospun PCL+gelatin nanofibers. *PLoS One*. 2016; 11: 1–12. <https://doi.org/10.1371/journal.pone.0154806> PMID: 27196306
43. Bashur CA, Dahlgren LA, Goldstein AS. Effect of fiber diameter and orientation on fibroblast morphology and proliferation on electrospun poly(d,l-lactic-co-glycolic acid) meshes. *Biomaterials*. 2006; 27: 5681–5688. <https://doi.org/10.1016/j.biomaterials.2006.07.005> PMID: 16914196
44. Hun C, Joon H, Hee I, Kang Y, Ae I, Park K-D, et al. Nanofiber alignment and direction of mechanical strain affect the ECM production of human ACL fibroblast. *Biomaterials*. 2005; 26: 1261–1270. <https://doi.org/10.1016/j.biomaterials.2004.04.037> PMID: 15475056
45. Teh TKH, Toh S, Goh JCH. Aligned Fibrous Scaffolds for Enhanced Mechanoresponse and Tenogenesis of Mesenchymal Stem Cells. *Tissue Eng Part A*. 2013; 19: 1360–1372. <https://doi.org/10.1089/ten.TEA.2012.0279> PMID: 23327653
46. Wang JH-C, Jia F, Gilbert TW, Woo SL-Y. Cell orientation determines the alignment of cell-produced collagenous matrix. *J Biomech*. 2003; 36: 97–102. [https://doi.org/10.1016/s0021-9290\(02\)00233-6](https://doi.org/10.1016/s0021-9290(02)00233-6) PMID: 12485643
47. James R, Kesturu G, Balian G, Chhabra AB. Tendon: Biology, Biomechanics, Repair, Growth Factors, and Evolving Treatment Options. *J Hand Surg Am*. 2008; 33: 102–112. <https://doi.org/10.1016/j.jhsa.2007.09.007> PMID: 18261674
48. Sharma P, Maffulli N. Basic biology of tendon injury and healing. *Surgeon*. 2005; 3: 309–316. [https://doi.org/10.1016/S1479-666X\(05\)80109-X](https://doi.org/10.1016/S1479-666X(05)80109-X) PMID: 16245649
49. Bosworth LA, Alam N, Wong JK, Downes S. Investigation of 2D and 3D electrospun scaffolds intended for tendon repair. *J Mater Sci Mater Med*. 2013; 24: 1605–1614. <https://doi.org/10.1007/s10856-013-4911-8> PMID: 23504088